Effect of composition on charge exchange, lattice expansion, and staging in potassium-ammonia graphite intercalation compounds

B. R. York and S. A. Solin
Department of Physics and Astronomy, Michigan State University, East Lansing, Michigan 48824-1116
(Received 9 October 1984)

We have studied the charge exchange and compositional dependence of the sandwich thickness of stage-1 alkali-ammonia ternary graphite intercalation compounds $K(NH_3)_xC_y$, $0 \leq x \leq 4.33$, $12 \leq y \leq 24$. A model of the sandwich energy is presented which explicitly accounts for x-dependent charge exchange and size or stiffness effects and is in excellent agreement with experimental measurements of the dependence of the (00l) x-ray diffraction patterns on ammonia vapor pressure. From this model we find that for the stage-1 compound $K(NH_3)_{4.33}C_{24}$, $f=0.95$ and that the NH_3 molecules solvate some of the electron charge which was originally donated to the carbon layers in the KC_{24} starting material. In addition, the NH_3 molecules form planar fourfold-coordinated $K(NH_3)_4$ clusters and hence also solvate the K^+ ions in graphite galleries. We suggest that the $K(NH_3)_4$ clusters together with "spacer" NH_3 molecules constitute the two-dimensional structural analog of the well-studied bulk, three-dimensional metal-ammonia solutions.

I. INTRODUCTION

Graphite is a prototypical layered solid in which the intralayer forces binding carbon atoms in a triangular planar lattice structure are much greater than the interplanar forces. This anisotropy in the interatomic forces makes it possible to intercalate graphite with many different chemical species. Intercalation is a process by which guest atoms, molecules, and/or ions are inserted into the interlayer spaces in the host graphite structure. The resulting graphite intercalation compound (GIC) shows a macroscopic expansion along the c-axis direction perpendicular to the carbon layer planes, which themselves remain essentially undistorted.

The most fundamental and intrinsically interesting characteristic of graphite intercalation compounds is their ability to form pure stages. Pure staging is characterized by the long-range *periodic* placement of intercalant layers between host graphite layers. For example, pure stage n designates the periodic insertion or intercalation of layers of atoms and/or molecules (intercalants) between n carbon layers with this stacking arrangement repeating over extended (>500 Å) distances. There is a charge transfer in the intercalation process between the intercalant layer and the graphite layers. Thus, in addition to characterization according to stage number, the intercalants in GIC's are also classified as donors or acceptors according to whether electron charge is transferred to or from the graphite sheets, respectively.

Detailed theoretical models outlining the physics of the staging phenomena have only recently been presented.[1-3] An important ingredient of those models is the contribution of the carbon-intercalant-carbon sandwich energy to the free energy, which establishes the equilibrium stage. The sandwich thickness d_s (which is the perpendicular distance between carbon layers that flank an intercalant layer) can be determined by minimizing the free energy with respect to d_s.

Safran and Haman[4,5] considered both elastic and electrostatic contributions to the sandwich energy. They concluded that the elastic contribution to the sandwich energy was the dominant mechanism for the kinetics of intercalation, while the electrostatic interactions were important in determining the equilibrium state or stage of the GIC. The recent model of Hawrylak and Subbaswamy[3] is somewhat similar to that of Safram (for modifications see Ref. 3 and references therein), but takes into account volume and in-plane intercalant density variations, and is capable of explaining experimentally observed effects[6,7] in binary alkali GIC's which had not been addressed in earlier models. A binary GIC is one in which a single chemical species has been intercalated into the galleries between the layers of the graphite host.

While a theoretical description of binary GIC's based on elastic and electrostatic energies can explain many experimentally observed phenomena, other effects which couple those energies are also significant. The coupling of elastic and electrostatic forces would be experimentally visible in a variation of d_s with composition and/or charge exchange (the amount of charge per intercalant exchanged between the intercalated species and the carbon sheets). Thus, any acceptable model of staging must adequately account for the variation in the sandwich thickness d_s with composition and charge exchange. To date, the experimental data necessary to test theoretical predictions for the variation of d_s with those parameters have been, at best, sparse. Furthermore, the composition of the binary alkali GIC's, which are the most widely-studied and well-understood GIC's, cannot be conveniently varied at constant stage. The variation in the composition at a fixed stage allows a more detailed study of the role of charge exchange in determining the sandwich energy. For example, Woo and co-workers[8] reported a small (0.3%) composition-dependent change in d_s for stage-2 LiC_{12} in comparison with stage-2 LiC_{18}, which they attribute to a competition between electrostatic and elastic effects.

Similarly, Metrot, *et al.*[9] noted a weak dependence of d_s on the amount of chemical overcharging of stage-1 H_2SO_4 GIC's, but chose to focus on the chemical aspects of their measurements rather than to explore in detail the coupling of d_s to the charge exchange f. It should also be mentioned that large variations ($\sim 10\%$) in d_s with composition x have been reported for the ternary GIC's $M_xM'_{1-x}C_8$,[10,11] where M and M' are alkali metals, but such variations are predominantly elastic in origin[10] and preclude a study of d_s versus f. A ternary GIC is one in which two distinct guest species simultaneously occupy the carbon interlayer space.

We have shown[12] that the K-NH_3 ternary GIC's permit an in-depth study of the variation of sandwich thickness d_s with composition and charge exchange f, at constant stage. The K-NH_3 intercalants form a two-dimensional (2D) liquid in the graphite galleries,[13] which represents a natural 2D counterpart of the well-studied[14–16] three-dimensional (3D) K-NH_3 solution. In particular, the M-NM_3 (M denotes alkali metal) GIC's offer the possibility of exploring the nonmetal-metal transition[17] in two dimensions. In view of this, it is interesting to note that several decades ago Rudorff and Schultze[18] prepared limited compositional forms of those compounds at low pressure, but they have only recently been investigated in detail.[13,19,20]

In this paper we will discuss and extend the coupled elastic energy-charge exchange model which has to date only been addressed in a preliminary report.[12] We will provide here new experimental details and additional physical insight into the K-NH_3 ternary GIC's. Finally, the approach taken here includes modifications that we feel provide a more global understanding of the K-NH_3 GIC's.

II. EXPERIMENTAL DETAILS AND RESULTS

All $K(NH_3)_xC_{24}$ samples were prepared by using a well-characterized stage-2 KC_{24} sample made in the usual manner[21] from the host material highly-oriented pyrolytic graphite (HOPG). The KC_{24} samples were rapidly transferred from their preparation vessel to another container, which was ultimately exposed to previously cleaned NH_3 gas. The transfer process was carried out in a Vacuum Atmospheres model no. MO-40-1 glove box maintained at <0.5 ppm $[O_2]/[H_2O]$ levels.

Many KC_{24} samples were prepared during the course of this work and their stoichiometry was carefully determined by accurately weighing the starting HOPG and the resultant intercalation compound. We found that the actual composition of the pure stage-2 compound was $KC_{24+\delta}$, where $-2.20\pm0.05<\delta\leq 0$. Nevertheless, we will follow custom and hereinafter often designate specimens by their nominal compositions, e.g., $K(NH_3)_xC_{24}$, but the actual composition will be used in any relevant analysis.

Commercial grade NH_3 (main impurities are 40 ppm O_2, 5 ppm H_2O) was purified by condensing it onto Na metal with liquid nitrogen. The NH_3 was then warmed to $-70\,^{\circ}C$ with a dry-ice—alcohol mixture. The solution was again frozen and any residual H_2 gas was pumped away. Hydrogen may be formed from the decomposition of NH_3 to the amide NH_2 by the reaction of NH_3 with impurities. This "freeze-pump-thaw" procedure[22] was repeated until there was no evidence of the evolution of H_2, determined by monitoring the pressure with a standard vacuum-thermocouple gauge.

Absorption isotherms or weight uptake measurements of KC_{24} for NH_3 gas were determined by two techniques. The first technique employed an archaic but quite useful device now referred to as a McBain balance.[23] This balance consisted of a very sensitive Hooke's-law quartz spring (force constant $k\approx 1$ mg/mm, equilibrium length $l_0\approx 30$ cm), that was calibrated with premeasured wire weights. The spring was vertically suspended from a specially-designed flange in a glove box with the low $[H_2O]/[O_2]$ levels indicated above. Extreme care was used in attaching the KC_{24} specimen (mass ~ 100 mg) to the base of the spring. A thick-walled glass tube designed to withstand >10 atm pressure was used to enclose the specimen-spring assembly and was connected to the flange through an O-ring Teflon coupling. The entire apparatus was removed from the glove box, connected to a vacuum system, and then exposed to clean NH_3 gas from a reservoir containing excess NH_3 liquid.

Vertical displacements from the KC_{24} equilibrium position which resulted from the intercalation of NH_3 vapor were monitored as a function of NH_3 pressure with a Wild model no. KM-326 cathometer with an accuracy of <0.05 mm or equivalently $<50\ \mu g$. By controlling the temperature of the excess liquid in the NH_3 reservoir, the ammonia gas pressure, P_{NH_3}, could be determined from the equation of state for the saturated vapor pressure of NH_3 (in atm), as a function of temperature[24] given in Eq. (1):

$$\log_{10}P_{NH_3}(T)=27.376\,004-\frac{1914.9569}{T}-8.459\,83\log_{10}T+2.393\,09\times10^{-3}T+2.955\,214\times10^{-6}T^2\,. \quad (1)$$

Corrections of the McBain balance data for buoyancy, significant only for $P_{NH_3}>1$ atm, were made by determining the density of NH_3 gas from the van der Waals equation of state[25] with P_{NH_3} given in Eq. (1), and the volume of the sample as follows: The area of the sample could be calculated from the weight, density, and d spacing or c-axis repeat distance of the host material HOPG. (Note that if the intercalant layers are disordered and/or unregistered with the graphite layers, then $d=[d_s+(n-1)3.35]$ Å, where n is the stage number and 3.35 Å is the interplanar distance in pristine graphite.) The volume of the specimen can then be determined from the d spacing of the NH_3 intercalated material, which in turn is obtained from $(00l)$ x-ray diffraction measurements. After the sample was initially intercalated with NH_3 at room temperature, the bulk composition of the specimen was reversibly varied over the range $1.49<x<4.33$ (where x is the mole ratio of NH_3 to K) for 10^{-3} atm $<P_{NH_3}<10$ atm. The McBain balance ab-

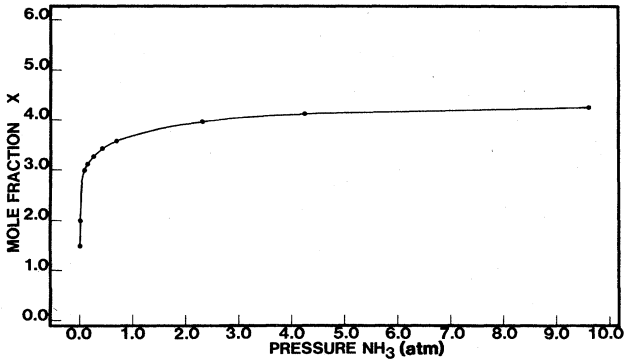

FIG. 1. Dependence of the mole fraction x (x denotes mole ratio of [NH_3]/[K]) of $K(NH_3)_xC_{24}$ with P_{NH_3}, determined by a McBain balance (Ref. 19) method. Experimental points are indicated by solid circles (●); the solid line is a guide to the eye.

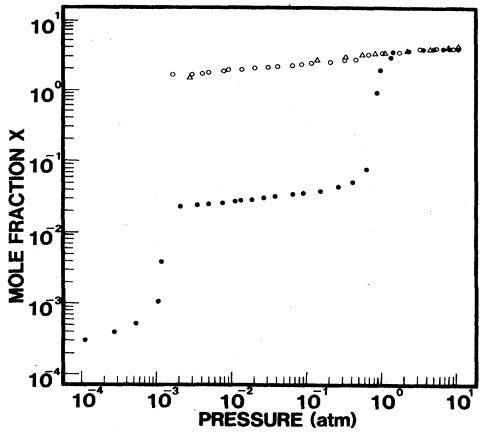

FIG. 2. Variation of the mole fraction x with P_{NH_3} for the ternary GIC $K(NH_3)_xC_{24}$ as measured by a "gas-handling" technique (see text). Experimental points indicated with a solid circle (●) represent the initial intercalation of NH_3; those with open circles (○) are for deintercalation. The McBain balance data from Fig. 1 have been replotted as open triangles.

sorption data, corrected for buoyancy, are shown in Fig. 1.

The second technique for weight-uptake measurements utilized a specially-designed high-pressure glass manifold, which was connected through a 3-mm Ace glass-Teflon valve to a vacuum system with an ultimate vacuum of 5×10^{-7} Torr. An NH_3 reservoir, a sample chamber, a standard volume, and a Datametrics Barocell type no. 590D-100P-3P1-H5X-4D capacitance manometer were also connected to the manifold each through a separate 3-mm glass-Teflon valve. The volume of the manifold and each chamber was determined by a series of expansions at a known initial pressure of an inert gas such as argon from the standard volume into a previously evacuated manifold or chamber. From a measurement of the final pressure resulting from the expansion, the volume of each chamber and manifold could be calculated and then averaged over several trials to yield an accuracy of $<1\%$. By monitoring the pressure difference before and after intercalation, together with the predetermined volumes, the number of moles of NH_3 taken in by the graphite can then be calculated from van der Waals equation.[25]

This "gas-handling" technique, the results of which are shown in Fig. 2 as solid circles for intercalation and open circles for deintercalation, complements the McBain balance technique, the data of which are also shown as open triangles in Fig. 2. The former allows access to the low-P, low-x region of the initial intercalation of KC_{24} with NH_3. In fact, for our typical samples (mass ~50 mg), the inclusion of the low-pressure region of Fig. 2 necessitated measuring the NH_3 content intercalated into graphite to an accuracy of 0.1 μmol. However, the "gas-handling" technique has a slightly higher error (1% versus 0.2%) compared with the McBain balance method at the high-pressure end. Note also that there was a small amount of adsorption of NH_3 onto the walls of the glass manifold that will affect the accuracy of x at low pressures ($<10^{-1}$ atm), but this was minimal and should not change the qualitative feature of the weight-uptake curve of Fig. 2.

All x-ray measurements and sample characterization reported here were accomplished utilizing a Huber model no. 430-440-512 four-circle diffractometer coupled through a vertically-bent graphite monochromator to a Rigaku 12-Kw rotating anode x-ray source equipped with a Mo anode. The x-ray signal from a Bicron NaI detector was fed into a Tracor-Northern 1710 multichannel analyzer (MCA). Both the MCA and Huber diffractometer were controlled using a DEC-PDP-1103 digital computer, with specially-designed software for automatically repeated scans along any predetermined path in real or reciprocal space.

In situ x-ray diffraction studies as a function of P_{NH_3} were also performed on the ternary GIC $K(NH_3)_xC_{24}$. A KC_{24} sample ($\sim0.7\times6\times10$ mm) prepared in the manner described above, was placed in an 8-mm Pyrex tube with excess liquid NH_3. The KC_{24} sample was initially intercalated with NH_3 at room temperature, and was found to be a pure stage-1 compound ($d=6.633$ Å) with a stoichiometry $K(NH_3)_{4.33}C_{24}$ determined by weight-uptake measurements. We then maintained the sample at room temperature for all subsequent measurements, but in order to change the sample composition, i.e., change x in $K(NH_3)_xC_{24}$, we varied the temperature of the excess NH_3 as follows.

A Dewar of ethyl alcohol was placed around the NH_3 end of the sample tube and the alcohol was slowly (≈20 K/h) cooled (to -110°C) to avoid exfoliation of the specimen. The ethyl alcohol was then replaced with liquid nitrogen as the low-temperature bath. The Dewar of liquid nitrogen was removed and a Dewar containing an ethanol slush at -110°C was placed over the NH_3 end of the sample tube and allowed to warm up slowly (~4.4 K/h) to room temperature. The ammonia pressure was again determined by monitoring the temperature of the excess NH_3 liquid and applying Eq. (1).

In situ x-ray (00l) diffraction scans were taken at 1-h intervals as the NH_3 warmed. Representative scans are shown in Fig. 3, which depicts the pressure evolution of the K-NH_3 GIC from stage 2 to stage 1. The pattern of

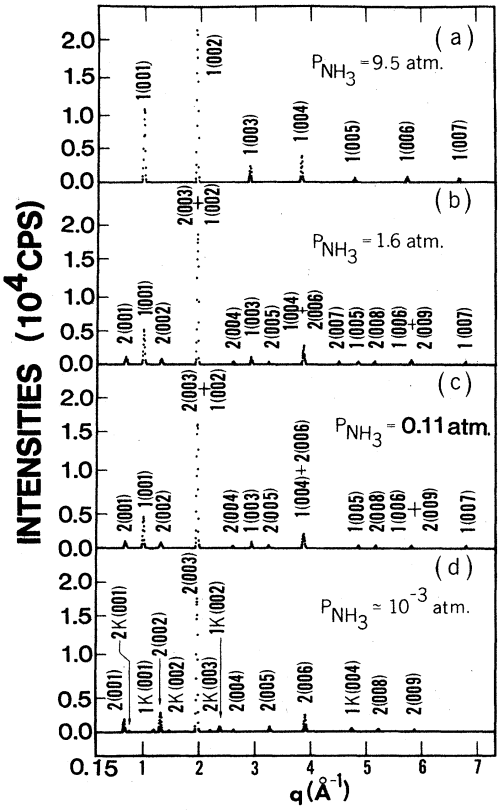

FIG. 3. (a)—(d) represent the P_{NH_3} evolution of the (00l) x-ray diffraction patterns of $K(NH_3)_xC_{24}$. Reflections associated with the stage-n K-NH_3 ternary GIC's are labeled n(00l). Those associated with the binary potassium GIC's are labeled nK(00l).

Fig. 3(d) is associated with a change in the color of the sample from dark metallic blue to a yellow-gold and reveals that the sample consisted of a mixed-phase system composed mainly of the stage-2 K-NH_3 ternary GIC with admixtures of the binary GIC's KC_{24} (d=8.67 Å) and

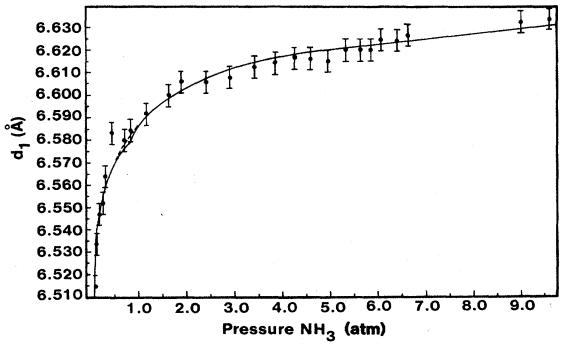

FIG. 4. Variation of the d spacing of stage-1 K-NH_3 GIC (d_1) with P_{NH_3}. The experimental points are shown as solid circles (●) with the indicated error bars, and the solid line represents a theoretical fit to the data using Eq. (18).

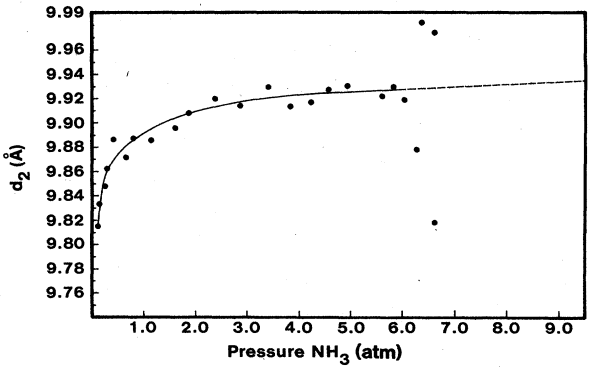

FIG. 5. Dependence of the d spacing of stage-2 (d_2) K-NH_3 GIC with P_{NH_3}. Experimental points are indicated with a solid circle (●), and the solid line is a guide to the eye. The dashed line is an extrapolation of the curve to P_{NH_3}=9.5 atm.

KC_8 (d=5.33 Å). The "yellowish" appearance of the sample surface is due to the presence of KC_8, which is normally gold in color. Observed reflections in each pattern are of instrument-limited width and thus, for the 1-mm slit settings used, indicate a c-axis correlation range of ~350 Å.

Shown in Figs. 4 and 5 are the d spacings of stage-1 (d_1) and stage-2 (d_2) K-(NH_3) GIC's as a function of P_{NH_3}. The NH_3 pressure dependence of the intensities of the (001) reflection of stage 1 and the (002) reflection of stage 2 is shown in Fig. 6 and clearly indicates a phase transition from stage 2 to stage 1 with increasing pressure. The inflections visible in the intensity data of Fig. 6 at P_{NH_3}=5.5 atm are due to compositional changes and will be discussed below. For P_{NH_3}>6.5 atm, only the (001) and (002) reflections of the stage-2 region are detectable in the (00l) x-ray diffraction patterns. The (003) reflection of stage 2 is masked by the strong (002) reflection of stage 1. The large fluctuations visible in d_2 versus P_{NH_3} of Fig. 5 are due to inaccuracies associated with determining d_2 from only the two observable low-angle reflections cited above. The dashed line in Fig. 5 is an extrapolation of the d_2 versus P_{NH_3} curve to P_{NH_3}=9.5 atm (corresponding

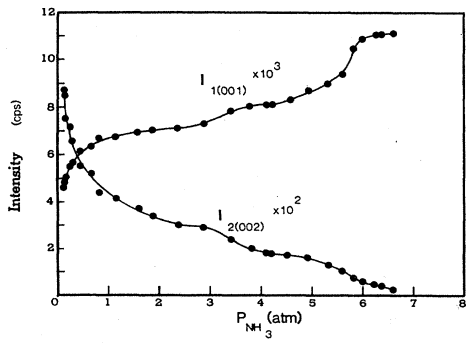

FIG. 6. Dependence of the intensities of the (001) reflection of stage-1 and the (002) reflection of stage-2 K-NH_3 GIC's with P_{NH_3} [indicated with solid circles (●)].

to T_{NH_3} equal to room temperature) with $d_2 = 9.930$ Å. Both the d spacings of Figs. 4 and 5 and the weight-uptake measurements of Figs. 1 and 2 show rapid changes for $P_{NH_3} < 1$ atm and establish that the c-axis expansion of the K-NH_3 GIC is due to the influx of NH_3.

III. DISCUSSION AND ANALYSIS

A. Comparison with Rudorff and Schultze's results on K-NH_3 GIC's

Before proceeding with the analysis of the above experimental data, it will be useful to discuss the stage-1 and stage-2 K-NH_3 GIC results of Rudorff and co-workers[18] in order that comparisons can be made with our results. It will also be necessary to discuss the physical implications arising from the weight-uptake curve of Fig. 2 and the x-ray diffraction pattern of Fig. 3(d) before a method of analysis can be established.

Rudorff and Schultze[18] showed, over 30 years ago, that metal-ammonia solutions (M-NH_3, where M is any alkali metal) could be readily intercalated into graphite. They prepared a stage-1 K-NH_3 GIC via two techniques. The first technique was to directly immerse the binary GIC KC_8 into liquid NH_3. They found that upon intercalation of NH_3, K was expelled from the specimen. A second technique was to directly immerse graphite powder in a metal-rich K-NH_3 solution. Both techniques, after the removal of excess absorbed NH_3 at 0 °C, were reported to yield the ternary GIC $K(NH_3)_{2.0}C_{12}$ with a d spacing of 6.5 Å. A stage-2 K-NH_3 GIC was also prepared by controlling the concentration of the K-NH_3 solution into which the graphite powder was immersed. Rudorff and Schultze[18] found, after the evacuation of NH_3, that only for a carbon/potassium molar ratio of 28 was a pure stage-2 compound formed with an average stoichiometry of $K(NH_3)_{2.3}C_{28}$ and d spacing of 9.9 Å.

From the results of Rudorff and co-workers, it seems energetically favorable at low NH_3 pressures for $K(NH_3)_xC_y$ GIC's to acquire a carbon/metal ratio of 12 for stage 1 and 28 for stage 2, and an NH_3 /metal ratio of 2.0 for both (stage 2 may have a slightly higher NH_3 /metal ratio). Thus, potassium was expelled from the binary GIC KC_8 upon submersion into liquid NH_3 according to the reaction

$$3KC_8 + 4(NH_3) \rightarrow 2KC_{12}(NH_3)_{2.0} + K \ . \quad (2)$$

Upon the removal of the absorbed NH_3 in a vacuum, both stage-1 and stage-2 K-NH_3 GIC's still retain large amounts of NH_3 ($x = 2.0$) in their respective galleries. Thus, at low pressures these K-NH_3 ternary GIC's are residue compounds.

We have also prepared pure stage-1 K-NH_3 GIC's in a manner similar to that of Rudorff and Schultz[18] (i.e., HOPG + K-NH_3 liquid and KC_8 + NH_3 liquid), except our samples have excess liquid NH_3 in the sample vessel. The (00l) x-ray diffraction patterns of KC_8 + NH_3 liquid and HOPG + K-NH_3 liquid are shown in Figs. 7(a) and 7(b), and indicate that the resultant stage-1 ternary GIC's have very similar d spacings of 6.516 and 6.586 Å, respectively. These values are in reasonable agreement with Rudorff and Schultze's results of $d = 6.5$ Å for both methods. Furthermore, our $KC_8 + NH_3$ liquid samples exfoliated upon intercalation, a process which appears to be as expulsion of potassium as reported by Rudorff and Schultze.[18] Nevertheless, it is reasonable to question whether the stoichiometry of our stage-1 compounds prepared from HOPG + K-NH_3 liquid and $KC_8 + NH_3$ liquid is in fact the same as reported by Rudorff and Schultze,[18] since at high NH_3 pressure it is possible to either expel potassium or intercalate additional ammonia.

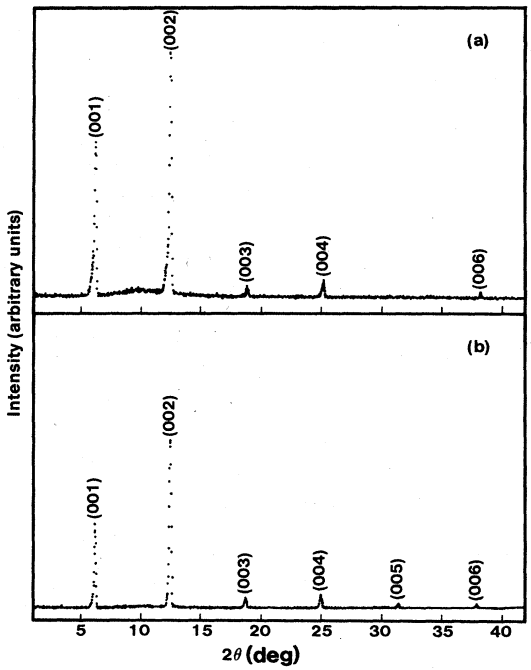

FIG. 7. Room-temperature (00l) x-ray diffraction patterns of (a) stage-1 KC_8+NH_3 liquid, and (b) stage-1 HOPG + K-NH_3 solution. The notation is the same as that of Fig. 3.

Given a fixed carbon/potassium ratio of 12, it is possible to estimate the maximum intercalation of NH_3 at 9.5 atm. The "effective" area of an NH_3 molecule can be estimated on the assumption that NH_3 completely fills the available area of the graphite gallery for stage-1 $K(NH_3)_{4.33}C_{24}$. The "available area" for the unit of composition $K(NH_3)_{4.33}C_{24}$ of stage 1 is $A = 56$ Å^2 and it was determined by subtracting the area of a potassium ion of radius 1.46 Å (see below) from the area of 24 carbon atoms. From $A = 56$ Å^2 and $x_{max} = 4.33$, the "effective area" of an NH_3 molecule, A_{NH_3}, is 13.07 Å^2, which following a similar analysis leads to a value $x_{max} = 2.0$ for the compound $K(NH_3)_xC_{12}$. Thus, if no potassium is ejected, the $K(NH_3)_xC_{12}$ compound becomes saturated at the low pressure (vacuum) at which $x = x_{max} = 2$ and ingests no more NH_3 even when P_{NH_3} is raised to 9.5 atm.

The d spacing of our stage-1 compounds prepared from HOPG + K-NH_3 liquid is ≈ 6.5 Å even with $P_{NH_3} \approx 9.5$ atm and lies very close to that reported by Rudorff and Schultze[18] ($d = 6.5$ Å). In contrast, our stage-1

$K(NH_3)_{4.33}C_{24}$ compound which was prepared by reacting KC_{24} with NH_3 has a d spacing of 6.633 Å. Therefore, it is indeed evident that large amounts of potassium are not expelled from the $K(NH_3)_xC_{12}$ system when it is exposed to elevated NH_3 pressures.

B. The absorption isotherm

We will now describe and explain the physical implications of the weight-uptake curve of Fig. 2 and the x-ray diffraction pattern of the residue compound of Fig. 3(d).

As P_{NH_3} is increased, the weight-uptake curve in Fig. 2 (solid circles) shows that little intercalation takes place until a pressure of 10^{-3} atm is reached, then rapid intercalation sets in. This rapid influx of NH_3 could be attributed to an activation energy associated with separating the graphite layers enough to allow a small amount of NH_3 to enter. For ammonia pressures $>10^{-3}$ atm a plateau region is reached with $x\approx 0.03$. This plateau region extends from 10^{-3} to 0.6 atm and is followed by another rapid influx of NH_3 reaching another plateau region at $x=4.0$. This transition at $P_{NH_3}=0.6$ atm is also concurrent with a stage transformation from stage 2 to stage 1 (refer to Fig. 6) and is accompanied by a dilution of the in-plane potassium density from KC_{12} to KC_{24}. At 9.5 atm the sample is a pure stage 1 with a stoichiometry of $K(NH_3)_{4.33}C_{24}$. As the pressure is lowered from 9.5 atm (open circles of Fig. 2), x now follows a new path and as $P_{NH_3}\rightarrow 0$, $x\rightarrow 1.49$, which is consistent with the fact that the compound which results from pumping off the NH_3 is a stage-2 residue compound.[18]

Akuzawa *et al.*[26] have also prepared K-NH_3 GIC's using quite different preparation techniques. They first prepared a stage-2 $K(NH_3)_{2.0}C_{28}$ using the methods of Rudorff and Schultze,[18] then evaluated the sample chamber at an elevated temperature and reintercalated to stage 1 with potassium vapor. Akuzawa and co-workers report a stage-1 compound with a d spacing of 5.4 Å, slightly larger than that of KC_8 of 5.35 Å and a stoichiometry from chemical analysis of $K(NH_3)_{0.03}C_6$. The exact composition of the samples prepared by Akuzawa *et al.* is somewhat in doubt, since NH_3 has a tendency to decompose at the elevated temperatures used to reintercalate potassium. The similarity in the K/NH_3 ratio $x=0.03$ of Akuzawa *et al.'s* sample and the x value of the first plateau region in Fig. 2 is striking in light of the totally different preparation techniques involved. This similarity indicates that once this first plateau region at $x=0.03$ is reached, the weight-uptake curve (see Fig. 2) is no longer reversible and subsequent desorption of NH_3 yields a stage-2 residue compound, $K(NH_3)_{0.03}C_{24}$.

Although we have not as yet measured the d spacing in that first plateau region of Fig. 2 at composition $K(NH_3)_{0.03}C_{24}$, we expect to find a carbon-intercalant-carbon sandwich thickness similar to that of $K(NH_3)_{0.03}C_6$, which according to Akuzawa *et al.*[26] is approximately $d=5.4$ Å as noted above. This similarity is not surprising since NH_3 sparsely populates the graphite galleries (for $x\approx 0.03$ the NH_3-NH_3 distances are ~ 100 Å) and graphite can easily accommodate a sufficiently small density of local elastic distortions (due to intercalation) without altering significantly its sandwich thickness.[27]

From the above discussion, a plausible explanation of the first rapid influx of NH_3 at 10^{-3} atm is as follows. The elastic energy of the carbon-(K-NH_3)-carbon sandwich is small since the sandwich thicknesses of $K(NH_3)_{0.03}C_{24}$ ($d_s\approx 5.4$ Å) and KC_{24} ($d_s=5.35$ Å) are nearly the same. Thus, even at these very low pressures, the NH_3 pressure is still sufficiently large to overcome the energy associated with creating sparsely-populated elastic distortions, thereby intercalating 0.03 moles of NH_3 per mole of K into the galleries. The plateau region of $x=0.03$ and the second rapid intercalation of NH_3 at $P_{NH_3}=0.6$ atm can be explained in a similar fashion. Since NH_3 has a high mobility in the galleries of graphite,[19] to significantly increase x beyond 0.03 may require the sandwich thickness on the average to be much larger (for example, $d_s\cong 6.5$ Å as measured on deintercalation at 0.6 atm) than that of $K(NH_3)_{0.03}C_{24}$ ($d_s\cong 5.4$ Å). Thus, the elastic energy involved with increasing x is large and the pressure to overcome this energy is also large. Therefore, x remains constant at $x\sim 0.03$ for several decades of ammonia pressure until rapid intercalation sets in at the critical pressure of 0.6 atm.

C. The residue compound $K(NH_3)_{1.49}C_{24}$

As noted above, the residue compound represented in the pattern of Fig. 3(d) contained three phases: stage-1 KC_8, stage-2 KC_{24}, and stage-2 $K(NH_3)_{1.49}C_{24}$. The bulk stoichiometry of the latter was established from the weight-uptake measurements shown in Figs. 1 and 2. These results at first glance are not consistent with the stoichiometry of the stage-2 residue compound $K(NH_3)_{2.3}C_{28}$ prepared by Rudorff and Schultze, but at this point it is not clear that such a comparison can be made given the difference in the initial conditions of sample preparation.

Since no potassium is expelled from $K(NH_3)_xC_{24}$ as x is reduced, the presence of KC_8 in the $x=1.49$ residue compound requires that for a fixed carbon/potassium ratio of 24 there must also exist expanded regions of KC_y where $y>24$. It is interesting to note that the formation of 75% of $K(NH_3)_2C_{28}$ is entirely possible just based on balancing the NH_3 content for the two compounds (i.e., 75% of $x=2.0\rightarrow x=1.5$). From the above observations it is possible to describe the three-phase system of Fig. 3(d) with the following reaction:

$$K(NH_3)_{1.49}C_{24}\rightarrow a\ K(NH_3)_xC_y+b\ KC_8+c\ KC_{24}\ . \qquad (3)$$

The relative magnitudes of a, b, and c and the mole fractions x, y can be determined by simultaneously solving the three mass equations 4(a), 4(b), and 4(c) that balance Eq. (3) for K, C, and NH_3, plus Eqs. 5(a) and 5(b), which represent the ratio of the intensity of the (003) reflection of $K(NH_3)_xC_y$ to the (002) reflection of KC_8, and the ratio of the (003) reflection of KC_{24} to the (002) reflection of KC_8, respectively:

$$1=a+b+c\ , \qquad (4a)$$

$$24=ay+8b+24c\ , \tag{4b}$$

$$1.49=ay\ , \tag{4c}$$

$$\frac{a\,|\,S_2'(q_{003}',x,y)\,|\,^2P_L(q_{003}')}{b\,|\,S_1(q_{002})\,|\,^2P_L(q_{002})}=\frac{I_2'(q_{003}')}{I_1(q_{002})}\ , \tag{5a}$$

$$\frac{c\,|\,S_2(q_{003})\,|\,^2P_L(q_{003})}{b\,|\,S_1(q_{002})\,|\,^2P_L(q_{002})}=\frac{I_2(q_{003})}{I_1(q_{002})}\ . \tag{5b}$$

Here q_{002}, q_{003}', and q_{003} are the wave vectors $[q=4\pi\sin(\theta)/\lambda]$ associated with the (002) reflection of KC_8, the (003) reflection of $K(NH_3)_xC_y$, and the (003) reflection of KC_{24}, respectively. Also shown in Eqs. 5(a) and 5(b) are the structure factors $S_1(q)$, $S_2'(q)$, $S_2(q)$ (which is also dependent on composition x,y) and the intensities $I_1(q)$, $I_2'(q)$, $I_2(q)$ for KC_8, $K(NH_3)_xC_y$, and KC_{24}, respectively, as well as the combined Lorentz polarization factor $P_L(q)$. Debye-Waller and absorption corrections were omitted from Eqs. 5(a) and 5(b) and are expected to produce only marginal differences in the results since $q_{002}\approx q_{003}$ and $q_{002}\approx q_{003}'$.

The parameters that result from simultaneously solving the above five equations are $a=0.71$, $b=0.24$, $c=0.05$, $x=2.1$, and $y=29.4$, which to within experimental uncertainty are consistent with $a=0.75$, $b=0.19$, $c=0.063$, $x=2.0$, and $y=28$, so that Eq. (2) can be rewritten in the following form:

$$K(NH_3)_{1.5}C_{24}=0.75K(NH_3)_{2.0}C_{28}+0.25KC_{12}\ ,$$

where

$$KC_{12}=0.75KC_8+0.25KC_{24}\ . \tag{6}$$

Equation (6) suggests that our stage-1 $K(NH_3)_{4.33}C_{24}$ sample evolved, as the pressure was decreased, to the stage-1 and stage-2 Rudorff and Schultze compositions given below:

$$K(NH_3)_{2.0}C_{24}=0.75KC_{28}(NH_3)_{2.0}+0.25KC_{12}(NH_3)_{2.0}\ . \tag{7}$$

This reaction is expected to occur at $P_{NH_3}\approx 10^{-2}$ atm, as estimated from Fig. 2 (i.e., for $P_{NH_3}\approx 10^{-2}$ atm, $x\approx 2.0$).

Upon further lowering of the ammonia pressure below 10^{-2} atm, a dynamic exchange of NH_3 between stage 1 and stage 2 and the environment may have caused the depletion of NH_3 in the stage-1 region yielding the unstable KC_{12} component which ultimately phase separated into KC_8 and KC_{24}.

A possible senario for the depletion of NH_3 in stage 1 is the following: As P_{NH_3} is lowered below 10^{-2} atm, the composition evolves to $x<2.0$; this is an energetically unfavorable situation for both stages. However, if as we show below, stage 2 has a higher affinity for NH_3 than does stage 1, it will "pull" the NH_3 across the graphite gallery from the stage-1 region. Then any excess in the stage-2 region, above $x=2.0$, will be desorbed. It has been established[13,15,16] that stage-1 $K(NH_3)_{4.33}C_{24}$ is a donor GIC, thus, Rudorff and Schultze's K-NH_3 compounds[18] are also likely to be donors. If a direct comparison can be made between ternary alkali-ammonia and binary alkali donor GIC's which have charge exchanges of $f\approx 1$ and 0.86 for the stage-2 and stage-1 compounds, respectively, then the charge on the potassium ion of stage-2 $K(NH_3)_{2.0}C_{28}$ is greater than that for stage-1 $K(NH_3)_2C_{12}$. A greater charge on the potassium ion results in a stronger charge—dipole bond with NH_3, which in turn requires that the stage-2 K-NH_3 GIC has a higher affinity for NH_3 than does stage-1. This would also explain the significantly higher NH_3/metal ratios of the other stage-2 alkali and alkaline earth NH_3 GIC's also reported by Rudorff and Schultze.[18]

D. The generalized reaction of KC_{24} with NH_3

From the above discussion it is likely that the compositions of the two stages are pressure dependent and Eq. (7) should be generalized in the following manner:

$$K(NH_3)_xC_{24}=p_1(NH_3)_{x_1}C_{y_1}+p_2K(NH_3)_{x_2}C_{y_2}\ , \tag{8}$$

where y_n, x_n, and p_n are the mole ratios of carbon/potassium, NH_3/potassium, and relative fraction of each stage n, all of which are pressure dependent and have yet to be determined.

To solve unambiguously for the above variables would require six independent equations. There are five equations that are readily at our disposal. These are the three mass equations that balance Eq. (8) for potassium, carbon, and NH_3, listed in Eqs. (9a), (9b), and (9c) below, plus the two intensity equations (10a) and (10b) for the (001) reflection of stage-1 $K(NH_3)_{x_1}C_{y_1}$ and the (002) reflection of stage-2 $K(NH_3)_{x_2}C_{y_2}$:

$$p_1+p_2=1\ , \tag{9a}$$

$$p_1y_1+p_2y_2=24\ , \tag{9b}$$

$$p_1x_1+p_2x_2=x\ , \tag{9c}$$

$$p_1\,|\,S_1(q_{001},x_1,y_1,\gamma_1)\,|\,^2P_L(q_{001})=\alpha I_1(q_{001})\ , \tag{10a}$$

$$p_2\,|\,S_2(q_{002},x_2,y_2,\gamma_2)\,|\,^2P_L(q_{002})=\alpha I_2(q_{002})\ . \tag{10b}$$

Again, we have purposely left out absorption and Debye-Waller corrections because such corrections will only marginally influence the results and inevitably complicate the analysis. The constant α should only depend on the x-ray scattering geometry. It was determined so that the slope of x_1 versus P_{NH_3} matched that of the weight-uptake measurements for $P_{NH_3}>6.0$ atm since, to a very good approximation, $P_1=1.0$ in that region (see Fig. 6). The notation used in Eqs. (9) and (10) is the following: q_{00l} is the wave vector associated with the $(00l)$ reflection of stage n, I_n and p_n are the intensities and fraction of each stage, $P_L(q)$ is the combined Lorentz polarization factor, and $S_n(q_{00l},x_n,y_n,\gamma_n)$ is the structure factor for stage n, which depends on the wave vector q_{00l}, the composition (x_n,y_n) and a charge exchange parameter (γ_n). Incorporated into the structure factors $S_n(q_n)$ are the charge exchange terms $f=1-\gamma_n(x_n-4)$, where $\gamma_2=0$ and $\gamma_1=0.424$ were inferred from NMR measurements[15] of $K(NH_3)_{4.33}C_{24}$. The charge exchange terms will be considered in more detail later.

In order to solve for the variables in Eqs. (9) and (10) as

a function of ammonia pressure an additional constraint is required. Such a constraint can be found by setting $x_2=2.3$. We have shown in earlier work[12] that x_2 is essentially pressure independent and $x_2=2.1$ at low pressures. However, small pressure-dependent compositional changes in y_1 and y_2 were not previously considered, but do not alter the basic pressure insensitivity of x_2. Therefore, since x_2 is pressure insensitive, y_2 can be expected to follow suit (this assumes of course that NH_3 completely fills the available gallery area determined by y_2).

Rudorff and Schultze reported that at very low ammonia pressures the stage-2 K-NH_3 ternary GIC had an average stoichiometry of $K(NH_3)_{2.3}C_{28}$,[18] which is consistent with our ternary GIC represented in Fig. 3(d). If y_2 remains constant at 28, we can estimate the value of $(x_2)_{max}$ by assuming that the stage-2 ternary GIC is maximally occupied by NH_3, that is NH_3 completely fills the available interlayer space. From the effective area of an NH_3 molecule previously calculated, we find $(x_2)_{max}=2.101$ for $y_2=23.512$, and $(x_2)_{max}=2.3$ for $y_2=28$. Therefore, to a good approximation x_2 is pressure independent and equal to 2.3.

With the above constraint, y_n and p_n, for each stage n, and x_1 can be determined by simultaneously solving Eqs. (9) and (10). This is accomplished by reducing these equations to a 6th-degree polynomial of one variable. The resulting solutions for the variations of y_1 and y_2 with P_{NH_3} are plotted in Fig. 8. It can be seen from Fig. 8 that as P_{NH_3} is increased, y_1 increases from Rudorff and Schultze's result of $y_1=12$ (open circles) to $y_1=24$, while y_2 remains relatively constant at Rudorff and Schultze's value $y_2=28$ (open circle at low pressure) until $P_{NH_3}<5.0$ atm, where it rises sharply. This sharp rise in y_2 for $P_{NH_3}\sim 5.0$ atm implies that our original assumption of the pressure insensitivity of y_2 is valid only in the range $P_{NH_3}\lesssim 5$ atm. However, our immediate concern is the pressure dependence of x_1. With the present approach, x_1 should be accurate up to $P_{NH_3}\lesssim 5.0$ atm and also for $P_{NH_3}\geq 6.0$ atm [see discussion of Eqs. (9) and (10)]. Thus, the sharp rise in y_2 does not pose a serious problem for determination of $x_1(P_{NH_3})$.

Small fluctuations of y_1 and y_2, visible in Fig. 8, are due to the artificial constraint of holding x_2 constant at 2.3, and can be largely removed by allowing small variations in x_2. The larger fluctuation in y_2 at $P_{NH_3}=3.2$ atm corresponds to an inflection in the intensities of the (001) reflection of stage 1 and the (002) reflection of stage 2 shown in Fig. 6. The dependence of the fractions p_1 and p_2 on P_{NH_3} deduced from the solutions of Eqs. (9) and (10) is shown in Fig. 9. The rapid changes in which $p_1\rightarrow 1$ and $p_2\rightarrow 0$ at $P_{NH_3}\approx 5.5$ atm are associated with the sharp rise of y_2 at that pressure. Furthermore, the dashed line indicates an extrapolation to $p_2=0.75$ and $p_1=0.25$ (at low NH_3 pressure) which would be consistent with the formation of the stage-1 and stage-2 Rudorff and Schultze compositions given in Eq. (6).

There are other indications that the value of y_2 should be in excess of 37 as indicated in Fig. 8. The room-temperature ($P_{NH_3}=9.5$ atm) (00l) x-ray diffraction patterns of $KC_{36}+NH_3$ liquid are shown in Fig. 10 and represent a two-phase system composed mostly of a stage-2 K-NH_3 ternary GIC, but with small amounts of a stage-1 K-NH_3 GIC. An analysis identical to that used on the three-phase system of Fig. 3(d) [see Eqs. (4) and (5)] was applied to determine the values of x_2 and y_2 for this two-phase system. It was found by assuming for stage 1, $y_1=24$ and $x_1=4.33$ and for stage 2 a maximally-occupied gallery, that $y_2=37.2$ (shown as a

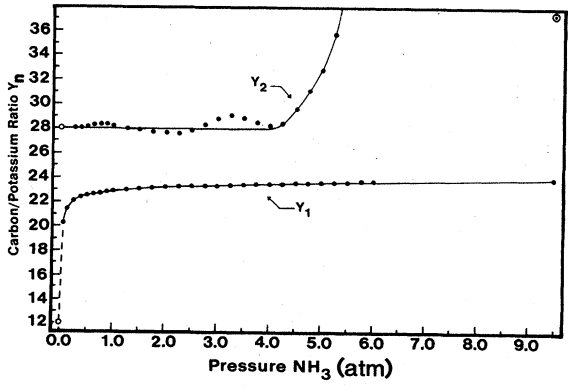

FIG. 8. Dependence on P_{NH_3} of the carbon/potassium ratios y_n for each stage-n K-NH_3 GIC. Analyzed data points are indicated with a solid circle (●). The solid lines are a guide to the eye. The dashed line for the y_1-versus-P_{NH_3} curve is an extrapolation to the Rudorff and Schultze (Ref. 18) C/K ratio $y_1=12$. The open circles represent the [C]/[K] ratios reported by Rudorff and Schultze (Ref. 18) for stage-1 and stage-2 K-NH_3 GIC's. The solid circle with a concentric circle (⊙) represents an estimate of y_2 at $P_{NH_3}=9.5$ atm based on an analysis of the x-ray data shown in Fig. 10 (see text).

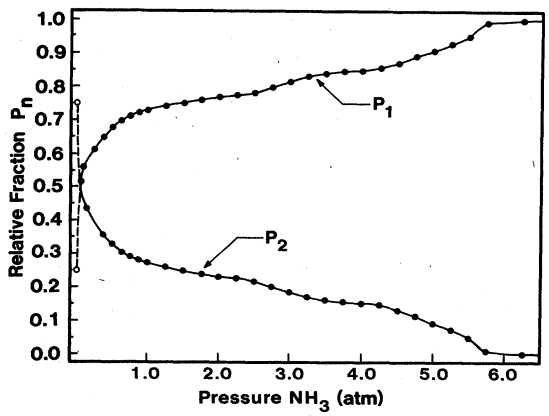

FIG. 9. Dependence of p_n, the fraction of each stage n on P_{NH_3}. Analyzed data points are indicated with a solid circle (●), and the solid line is a guide to the eye. The dashed line indicates an extrapolation from the p_n-versus-P_{NH_3} curves to the values of $p_1=0.25$ and $p_2=0.75$ at $P_{NH_3}\approx 0$ atm (indicated with open circles), which would be consistent with the formation of the stage-1 and stage-2 Rudorff and Schultze (Ref. 18) K-NH_3 GIC's [see Eq. (7) of the text].

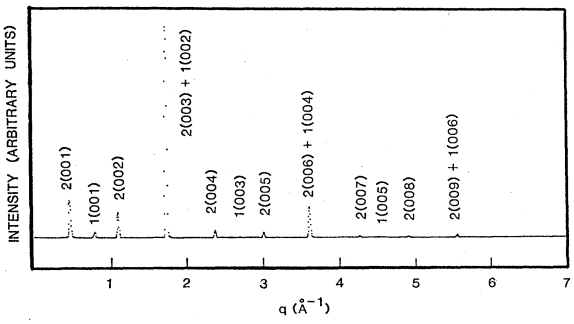

FIG. 10. Room temperature ($P_{NH_3}=9.5$ atm) ($00l$) x-ray diffraction pattern of $KC_{36}+NH_3$ liquid. The notation is the same as that of Fig. 3.

solid circle with a concentric open circle in Fig. 8), which may indicate that at $P_{NH_3}\approx 9.5$ atm, $K(NH_3)_{3.2}C_{37}$ is a pure stage-2 K-NH_3 GIC.

E. x_1 versus P_{NH_3} and the Fowler-Guggenheim form

Figure 11 shows the variation with P_{NH_3} of x_1 (solid circles) for $K(NH_3)_xC_{24}$ and the corresponding fit to a Fowler-Guggenheim (FG) adsorption equation[23] (solid line in Fig. 1) given below

$$P_{NH_3}=\frac{\alpha x_1}{(\beta-x_1)}e^{\omega x_1}\ , \tag{11}$$

with

$$\alpha=0.496\times10^{-5}\pm0.077\times10^{-5}\ ,$$

$$\beta=4.40\pm0.06,\quad \omega=2.43\pm0.04\ .$$

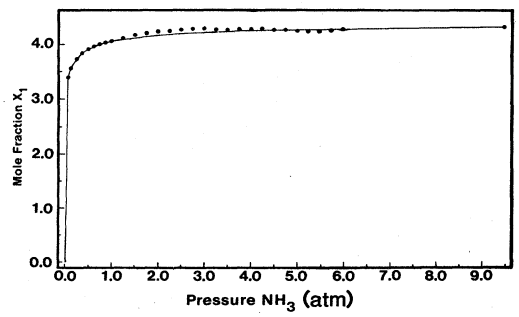

FIG. 11. Variation of the mole fraction of stage-1 x_1 with P_{NH_3}. Analyzed data points are indicated with solid circles (●). The solid line represents a least-squares fit to x versus P_{NH_3} using Eq. (11) of the text with $\alpha=0.496\times10^{-5}$, $\beta=4.40$, and $\omega=2.43$.

It is interesting to note that because the carbon/potassium ratios have been allowed to vary, the FG function now provides a better fit to the data of Fig. 11 than does the Langmuir function[28] which was previously applied.[12] The superiority of the FG form is not surprising since the Langmuir function is a zero-order approximation to adsorption and does not include the interaction between adsorbed atoms. However, the Fowler-Guggenheim equation given above includes this interaction and reduces to the Langmuir form where $\omega=0$.

The fit of x_1 versus P_{NH_3} shown in Fig. 11 yields the parameter ω which measures the interaction energy between NH_3 molecules. Fowler and Guggenheim derived the relation $\epsilon=\beta kT\omega/Z$, where for our use Z is the number of nearest-neighbor NH_3 molecules. The interaction energy between NH_3 molecules is ϵ, kT is the usual thermal energy, and β and ω are given above, with $\omega>0$ indicating a repulsive interaction between molecules. We find $\omega>0$ and for a maximum close-packed structure of six nearest neighbors $\epsilon_{min}=+0.04$ eV.

An estimate can be made of the maximum repulsive energy of two interacting dipoles from $\epsilon_{max}=\mu^2/r^3$.[29] Here, μ is the dipole moment and we have taken r as the close-packed hard-sphere diameter of the NH_3 molecule. By using the known value for $\mu_{NH_3}=1.5$ D (Ref. 25) and $r=3.41$ Å from diffuse x-ray scattering measurements of liquid NH_3,[30] we find $\epsilon_{max}=0.035$ eV which is, within error, in agreement with the repulsive energy found from the parameter ω.

A repulsive interaction between NH_3 molecules is contrary to physical intuition, since one would expect dipole alignment to be energetically favorable. However, it is known from NMR results[19] that the NH_3 threefold axis which is the dipole axis is dynamically tilted toward the potassium ion to which it is bound, thereby restricting the molecule's ability to orient itself. There are also steric constraints on the NH_3 molecule which are imposed by the graphite lattice as can be seen from Fig. 12. The in-

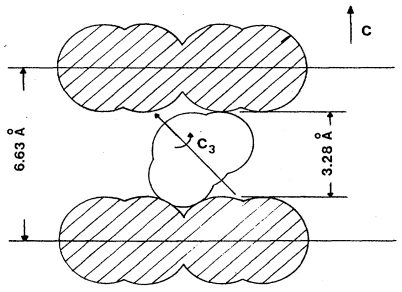

FIG. 12. In-plane view of the surface of revolution of an NH_3 molecule about its C_3 axis in a plausible configuration in the stage-1 $K(NH_3)_{4.33}C_{24}$ sandwich. All atomic sizes are scaled relative to their van der Waals radii (Ref. 21): $r_C=1.675$ Å, $r_N=1.5$ Å, and $r_H=1.2$ Å. Rotations about the C_3 axis cause the three hydrogens to form an annular ring. This ring is placed in the hexagonal cavity of carbon atoms with the C_3 axis tilted with respect to the c axis of graphite. The carbon atoms of the graphite bounding planes are shaded.

ability of the NH_3 molecule to freely orient means that the probability for dipole-dipole alignment is low and that the dipole-dipole interaction could be repulsive. The accuracy of the magnitude of the interaction energy derived from Eq. (11) is not high, but its repulsive character ($\omega > 0$) is unambiguous.

F. The model

We now focus on the theoretical model which we have used to fit the dependence of the sandwich thickness or d spacing of stage-1 $K(NH_3)_{x_1}C_{y_1}$ on P_{NH_3}. In addition, we will present experimental details and physical insight into the properties of the K-NH_3 ternary GIC, which have not been discussed in our earlier work.[12]

It is known that for GIC's the intercalant-intercalant interaction can be mediated by elastic strain fields.[4,5] The balance between the local distortions which are produced by intercalation and which give rise to these elastic strain fields and the forces that bind the carbon layers together determines the c-axis repeat distance and sandwich thickness of the resulting GIC. To describe the K-NH_3 ternary GIC sandwich, we have used a harmonic model in which the carbon sheets of pristine graphite which initially are "connected" by springs of force constant k_0 with equilibrium length d_0 are intercalated by the "insertion" of two additional springs representing K and NH_3 with force constants k_K and k_A and equilibrium lengths d_K and $d_A > d_0$.

The K-NH_3 intercalant of the stage-1 ternary GIC has been established to be of the donor type from x-ray measurements of the a-axis lattice parameter[13] and from NMR (Ref. 19) and reflectivity measurements.[20] Most of the charge donated by potassium remains on the carbon sheets after NH_3 insertion, and for the purposes of this discussion we assume that this charge is distributed uniformly, leaving behind a positively-charged K-NH_3 layer which is "sandwiched" between negatively-charged carbon sheets. In actuality, for donor compounds such as the alkali GIC's it has been shown[31] that the charge on the carbon layers is not completely delocalized, but screens the positive ions by accumulating around them. The carbon layers are also not rigid sheets, but can accommodate distortions perpendicular to the layer.[27] Nevertheless, a model which describes the K-NH_3 ternary sandwich as uniformly charged rigid carbon sheets separated by "atomic" springs, constitutes a sufficiently reasonable approximation to provide useful information. Following Hawrylak and Subbaswamy[3] and Dahn *et al.*[32] the stage-1 sandwich energy E per carbon atom can be expressed as

$$E = -\alpha x_K^{3/2} + \Omega d_{s_1} x_K^2 f^2 + \tfrac{1}{2}k_0(d_{s_1} - d_0)^2 + \tfrac{1}{2}x_K k_K (d_{s_1} - d_K)^2 + \tfrac{1}{2}x_A k_A (d_{s_1} - d_A)^2 . \quad (12)$$

Here α and Ω are constants, d_{s_1} is the equilibrium sandwich thickness of stage 1, and x_K and x_A are the concentrations of K and NH_3 in units of the number of carbon atoms, i.e., $x_K = N_K/N_C$ and $x_A = N_A/N_C$, where N_J is the number of atoms of type J in the bulk specimen for a particular stage.

In Eq. (12) the first term represents the binding or cohesive energy of a 2D free-electron gas, while the second term is the electrostatic energy associated with separated layers of charge. The remaining terms represent the elastic energies associated with pure graphite ($x_K = x_A = 0$) and potassium ($x_A = 0$, $x_K \neq 0$) and ammonia ($x_K = 0$, $x_A \neq 0$) GIC's. The equilibrium length d_K for the potassium intercalant is related to the size of the K species which in turn depends on the charge transfer f from the potassium ion to the carbon sheets through the relation[33]

$$r_K = f r_{K^+} + (1-f) r_{K^0} , \quad (13)$$

where r_K is the radius of the K ion with charge exchange f, and r_{K^+} and r_{K^0} are the ionic and atomic radii of potassium. Enoki *et al.*[33] have used this relationship to determine the size of K and Rb ions in alkali binary GIC's, and were able to explain the differences they observed in the ESR signals of hydrogenated KC_8 and RbC_8. In order to relate r_K in Eq. (13) to d_K, the ionic and atomic equilibrium lengths (or sandwich thicknesses) d_{K^+} and d_{K^0}, respectively, must be established. To a very good approximation d_{K^0} and d_{K^+} can be determined from the following relations:

$$d_{K^0} = 2r_{K^0} + R_0 , \quad (14a)$$

$$d_{K^+} = 2r_{K^+} + R_0 , \quad (14b)$$

where the geometrical factor $R_0 = 2.69$ Å was obtained from the experimental value of $d_{K^+} = 5.35$ Å with $r_{K^+} = 1.33$ Å.[33] Using Eqs. (14a) and (14b), Eq. (13) can be rewritten as

$$d_K = f d_{K^+} + (1-f) d_{K^0} , \quad (15)$$

where

$$d_K = 2r_K + R_0 .$$

It can be expected that the charge exchange f in Eq. (15) is dependent on the NH_3 concentration x_A, since it is well known[14–16] that NH_3 in metal-ammonia (M-NH_3) solutions has a strong affinity for electrons. Therefore, it is useful to review briefly below the properties of bulk 3D metal-ammonia solutions which elucidate the relationship between f and x_A in the 2D analog $K(NH_3)_xC_{24}$.

As alkali metal is added to liquid NH_3 to form a dilute 3D M-NH_3 solution[14,15] the metal relinquishes its valence electron to the liquid NH_3 and (for M equals potassium) is solvated or surrounded by six octahedrally coordinated NH_3 molecules. Solvation of the expelled electron also occurs, and it forms what will be referred to as an electron cage with surrounding NH_3 molecules. However, the number of NH_3 molecules required for electron-cage formation on the basis of energy considerations is not known exactly, but is estimated to be between four and six.[34] Ammonia is bound in $M(NH_3)_6$ complexes by charge-dipole forces, with each NH_3 molecule oriented so that its dipole points away from the metal ion. In contrast, the binding of NH_3 in electron cages is much weaker. Copeland *et al.*[34] have shown that electron-cage formation may

be brought about by the self-trapping of an electron in a cavity produced by NH_3 molecules through short-range interactions with NH_3 dipoles and by the long-range polarization of the NH_3 medium. When the metal concentration is increased enough to allow significant overlap in the wave functions of the individual electron cages, electron "hopping" from cage to cage occurs and a nonmetal to metal transition takes place.

According to the Mott criterion,[35] the critical electron concentration n for a nonmetal-metal transition is $n^{1/3}a_H \approx 0.25$, where a_H is the effective hydrogenlike radius of the electron cage. For K-NH_3 solutions, the nonmetal-metal transition occurs at ≈ 4 mol% metal [MPM equals moles of metal/(moles of metal plus moles of NH_3)$\times 100\%$). Increasing the metal concentration eventually leads to an insufficient amount of NH_3 molecules with which to solvate the expelled valence electron of the metal. For example, in the very dilute region, MPM $< 10^{-5}$, there is essentially an infinite number of NH_3 molecules for each electron, but at ten MPM there are only nine NH_3 molecules for each metal ion. Assuming six NH_3 molecules are bound to the metal ion, only three can couple to the electron. Thus, at high concentrations the expelled valence electrons which cannot be solvated are forced into the conduction band, causing the M-NH_3 solution to behave as a liquid metal. In fact it has been shown[36] from reflectivity experiments that there is a gradual transition between electron-cage formation and the conduction-band regime. Also note that solvated cations and solvated electrons may interact to produce neutral species[37,38] either by direct cation-electron interaction, in which there are no NH_3 molecules in between their respective centers, or by NH_3-shared ion-electron pairs, in which the solvated cation and solvated electron share one or more NH_3 molecules, but still retain their own identities.

It is clear from the above discussion that the amount of electron solvation in M-NH_3 solutions depends on the relative concentration of NH_3 to that of K which can be written as X, where $X = x_A/x_K$. There also exists a minimum concentration X_c below which electron solvation cannot occur.

As noted above, Rudorff and Schultze showed several decades ago that metal-ammonia solutions could be intercalated into graphite.[18] It is surprising that neither the structural or molecular form of the intercalant, nor its 2D metal-ammonia character as compared with a 2D nonmetal-metal transition, have yet been explored.

The metal hexamine $K(NH_3)_6$ cannot be intercalated into graphite, since that would require a sandwich thickness of at least 10 Å and the maximum value observed for the K-NH_3 ternary GIC's is 6.6 Å. However, if a pair of NH_3 molecules which lie on the same fourfold octahedral axis of $K(NH_3)_6$ are removed, leaving a planar fourfold-coordinated $K(NH_3)_4$ cluster, intercalation is possible. Given an interlayer space of 3.28 Å, which is defined to be the difference between the carbon-K(NH_3)-carbon sandwich thickness and the van der Waals diameter of the carbon atoms that flank an intercalant layer, only a monolayer of NH_3 can occupy the interlayer gallery. This point is illustrated in Fig. 12. It is interesting to note that fourfold coordination is also suggested by weight-uptake measurements of stage-1 $K(NH_3)_{4.33}C_{24}$, with the 0.33 NH_3 "spacer" molecules per $K(NH_3)_{4.0}$ cluster possibly involved in electron-cage formation. In principle, other planar N-fold coordination possibilities exist with $N = 2,3,5,6$. However, such N-fold configurations are very unlikely because of steric limitations and/or the fact that the potassium-NH_3 components do not adopt such planar arrangements in bulk M-NH_3 solutions. Moreover, only fourfold coordination is consistent with recent in-plane diffuse x-ray scattering experiments on $K(NH_3)_xC_{24}$.[13]

The entrance of NH_3 into the graphite galleries results in the solvation of both potassium and of electrons originally donated by potassium to the graphite layer. The electron solvation is a manifestation of the collateral extraction of charge out of the carbon sheets together with the formation of electron cages. For the most dilute case, which corresponds to stage-1 $K(NH_3)_{4.33}C_{24}$, the concentration of potassium relative to NH_3 is still equal to 19 MPM, well into the metallic region of a bulk 3D M-NH_3 solution with the same concentration. Thus, it is very likely that the K-NH_3 intercalant layer acts as a 2D liquid metal with delocalized electrons, which are collectively shared by each potassium ion.

From the above discussion, it can be expected that as NH_3 is added to KC_{24}, little if any electron solvation takes place, since NH_3 preferentially solvates the available potassium ions until a critical concentration $X_c = 4.0$ is exceeded. It can be assumed to a first approximation and for simplicity that the charge exchange f varies linearly with the excess NH_3 above $X = X_c$. Thus,

$$f = \begin{cases} 1 & \text{for } X < X_c \ , \\ 1-\gamma(X-X_c) & \text{for } X > X_c \ , \end{cases} \tag{16}$$

where $X_c = 4.0$ and the constant γ has yet to be determined.

By incorporating Eqs. (15) and (16) into Eq. (12) and minimizing the sandwich energy E with respect to the sandwich thickness d_{s_1} for a given x_K and x_A we find:

$$\frac{d_{s_1}}{d_{K^+}} = \frac{\left[1+X_c\frac{k_0}{x_K k_K}\frac{d_0}{d_{K^+}}+X_c\gamma\left[1-\frac{d_{K^0}}{d_{K^+}}\right]\right]+\left[\frac{k_A}{k_K}\frac{d_A}{d_{K^+}}\gamma\left[\frac{d_{K^0}}{d_{K^+}}-1\right]\right]X_1}{1+\frac{k_0}{x_K k_K}+\frac{k_A}{k_K}X_1} + \frac{\Omega x_K[1-\gamma(X_1-X_c)]^2}{k_K\left[1+\frac{k_0}{x_K k_K}+\frac{k_A}{k_K}X_1\right]} \ . \tag{17}$$

When pristine graphite is intercalated with potassium and ammonia, the resultant carbon interlayer distance increases by about a factor of 2. As a result of this large expansion the carbon force constant k_0 appropriate to Eq. (17) is not equal to that of pure graphite. In order to properly determine k_0 and k_K in Eq. (17), a microscopic theory with appropriately chosen interaction potentials would have to be constructed and the force constants evaluated. However, a crude approximation can be made for k_0 by describing the carbon-carbon interlayer interaction with a Lennard-Jones potential, the minimum of which is at $r_0=3.35$ Å, the interlayer distance in pristine graphite, and calculating the force constant (curvature) at $r=6.63$ Å, the interlayer distance in $K(NH_3)_{4.33}C_{24}$. Using this approach, we estimate that k_0 for $K(NH_3)_{4.33}C_{24}$ is a factor of ~ 200 smaller than that of pristine graphite. Similarly, we find that the value of k_K appropriate to $K(NH_3)_{4.33}C_{24}$ decreases only about a factor of 2 from that for KC_{24} which is not surprising since the sandwich thickness of $K(NH_3)_{4.33}C_{24}$ is only about 20% larger than d_{K^+}. The above method for estimating force constants is of course oversimplified and ignores effects such as charge exchange, which would tend to decrease even further the interlayer interaction. Thus, it is clear that to a good approximation $k_0/k_K x_K \ll 1$, and that the value of k_K may be approximately determined from those measured for the potassium GIC's.

It should also be mentioned that the results of Hawrylak and Subbaswamy[3] for KC_x are also consistent with $k_0/k_K x_K \ll 1$. In addition, they found that the electrostatic contribution to d_s [second term in Eq. (17)] is quite small and we also find it to be negligible. With $\Omega \approx 0$ and $k_0/k_K x_K \ll 1$, Eq. (17) can be rewritten:

$$\frac{d_{s_1}}{d_{K^+}} = \frac{\left[1-\gamma X_c\left[\frac{d_{K^0}}{d_{K^+}}-1\right]\right]+\left[\gamma\left[\frac{d_{K^0}}{d_{K^+}}-1\right]+\frac{k_A}{k_K}\frac{d_A}{d_{K^+}}\right]X_1}{1+\frac{k_A}{k_K}X_1}, \tag{18}$$

where $X_c=4.0$.

The force-constant ratio k_A/k_K of the K-NH_3 GIC in Eq. (18) can be estimated from measurements of bulk potassium and bulk ammonia. The bulk compressibilities of the alkali metals K, Rb, and Cs, and of NH_3 are at least an order of magnitude higher than that of pristine graphite. Therefore, a c-axis compression of the GIC sandwich results primarily in a deformation of the intercalant in K-NH_3 GIC's. The effective c-axis force constant of the sandwich can thus be approximated by the interatomic force constants determined from measurements of the bulk properties of the intercalants. For example, the c-axis force-constant ratio determined from neutron scattering experiments[39] on KC_8 and RbC_8 is, within experimental error, equal to the value $k_K/k_{Rb}=1.46$ obtained from ultrasonic measurements of the room-temperature elastic constants of bulk potassium and rubidium metal.[40]

From the compressibility of liquid potassium[41] (C_K) and liquid NH_3 (Ref. 15) (C_A) we find an approximate force-constant ratio $(k_A/k_K)\sim(C_A/C_K)^{-1}=0.56$. In addition, from the longitudinal sound velocities v_i for liquid potassium[41] and for NH_3 (Ref. 15) determined by ultrasonic measurements and the relation[42] $v_i=(k_i/\rho_i)^{1/2}$, where ρ_i is the density of the liquid species i, the force-constant ratio is found to be $k_A/k_K=0.77$.

An independent estimate of the force-constant ratios k_A/k_K can be made from an expression given by Dresselhaus *et al.*[39] By fitting the phonon dispersion curves of several GIC's, they found an empirical relation between the force constant of an intercalant and the corresponding equilibrium sandwich thickness. Their result can be rewritten to determine the force-constant ratio k_A/k_K as a function of d_A (defined above) and the in-plane intercalant density S. Thus,

$$\frac{k_A}{k_K}=\frac{17.11}{S}e^{-d_A/4.48}. \tag{19}$$

Equation (19) was derived using a value of $k_K=2.3$ (Ref. 39) (normalized to k_0 of pristine graphite). To our knowledge NH_3 cannot be solely intercalated into graphite, therefore, we must estimate the values of d_A and S to be used in Eq. (19).

We know from recent NMR measurements[19] of stage-1 $KC_{24}(NH_3)_{4.33}$ that the NH_3 molecule is rapidly rotating (on NMR timescales) about its c_3 axis which simultaneously precesses about the graphite c axis (see Fig. 12). The motion of the NH_3 molecule is nevertheless constrained (i.e., it does not tumble freely) by the charge-dipole forces which bind it to the potassium ion and by steric forces imposed by the bounding graphite planes. In a fictitious binary "NH_3-GIC" the NH_3 molecules could freely rotate in the graphite galleries. Free rotations of the NH_3 molecules can be ensured if the molecule occupies a volume determined by inscribing its surface of revolution about the c_3 axis (see Fig. 12) in a sphere of radius $r_{NH_3}=2.14$ Å. If such a sphere fits precisely into the double hexagonal cavity of the bounding graphite planes, the resultant value of d_A would be $d_A=7.08$ Å. With that value of d_A and $S=5.46$ established from the in-plane area $\pi r_{NH_3}^2$, we find from Eq. (19) that $k_A/k_K=0.65$. This value of $k_A/k_K=0.65$ is in excellent agreement with those obtained from measurements of the GIC compressibilities ($k_A/k_K=0.56$) and of the sound velocities of the intercalants K and NH_3 in bulk form ($k_A/k_K=0.77$), and constitutes the average of those measurements. We will, therefore, assume for the remainder of this paper that $k_A/k_K=0.65$.

G. Comparison with experiment

We have fit d_1 versus P_{NH_3} in Fig. 4 ($d_{s_1}=d_1$ for stage 1) using the Fowler-Guggenheim form of x_1 versus P_{NH_3} [see Eq. (11)], $k_A/k_K=0.65$, and Eq. (18), with only two adjustable parameters, which are the terms within large brackets in the numerator of Eq. (18). The results of that fit are shown as a solid line in Fig. 4 and constitute excellent agreement between theory and experiment. The apparent cusp in the fit of d_{s_1} versus P_{NH_3} at $P_{NH_3}<1$ atm is expected, since we have assumed a charge exchange f that inherently has a discontinuity in slope at $x=4.0$. This cusp is unphysical and should be smoothed (see dashed line in Fig. 4). From the fit of Eq. (18) to our data we find directly $\gamma=0.143\pm0.013$ and $d_A=7.05\pm0.04$ Å. The value of $d_A=7.05$ Å is surprisingly close to our estimate of $d_A=7.08$ Å which indicates a self-consistency in our approach. From $\gamma=0.143$ we find for stage-1 $K(NH_3)_{4.33}C_{24}$ the charge exchange $f=0.95$ which, given the uncertainty in determining f by any method, is in reasonable agreement with values obtained from measurements of reflectivity,[20] $f=0.73$ and NMR,[19] $f=0.86$. It should be mentioned that different values of k_A/k_K were tried and the resultant value of f was insensitive to the choice of k_A/k_K, i.e., $f\approx0.95$ for $0.3<k_A/k_K<0.9$, but a least-squares fit with $f=1.0$ could not be obtained.

The agreement between the charge exchange f obtained from NMR and reflectivity measurements, and that extracted from the fit of d_{s_1} versus P_{NH_3}, can be improved by considering other mechanisms for electron solvation such as NH_3 shared ion-electron pairs. That is, it is possible for the NH_3 molecules of different fourfold K-NH_3 clusters to orient themselves to form a cavity in which they can bind an electron. This would imply that for $X<X_c$ (where presently $X_c=4.0$) the charge exchange $f<1$. It is probable that f varies nonlinearly with the number of fourfold K-NH_3 clusters. This nonlinearity could be treated by adding additional terms and parameters to Eq. (16) or equivalently to Eq. (18). This would marginally improve the fit to the data of Fig. 4. However, such a procedure is not warranted because Eq. (18) contains the essential physics of the charge exchange process and the data of Fig. 4 does not vary rapidly enough with P_{NH_3} to allow additional parameters to be accurately determined.

For the purposes of illustration, let us assume that the current description of the charge exchange f given in Eq. (16) is applicable, but because of the existence of other electron solvation mechanisms the constraint $X_c=4.0$ must be relaxed to permit smaller values of X_c. From the current fit of d_{s_1} versus P_{NH_3} in Fig. 4, we find $\gamma X_c=0.57$, and for a charge exchange $f=0.80$ we estimate that $X_c=3.2$. This indicates that the inclusion of other solvation mechanisms tends to lower X_c and brings the extracted charge exchange f into better agreement with values determined in other measurements.

From the parameter

$$(d_A/d_{K^+})(k_A/k_K)+\gamma(d_{K^0}/d_{K^+}-1)=0.908$$

and $\gamma=0.143$, obtained from the fit to d_1 versus P_{NH_3}, we estimate that the relative elastic contribution of the charge transfer term $\gamma(d_{K^0}/d_{K^+}-1)$ to the sandwich expansion is at least 6%. Furthermore, the fractional increase in the sandwich thickness of our stage-1 $K(NH_3)_{4.33}C_{24}$ ($d=6.633$ Å) relative to Rudorff and Schultze's stage-1 $K(NH_3)_{2.0}C_{12}$ ($d=6.5$ Å) is 2%, which can be fully accounted for by a charge transfer coupled elastic expansion. As a final point, x_2 is pressure insensitive (at least at low pressure); therefore, the variation of d_2 with P_{NH_3} (see Fig. 5) must depend more on the variation with x_1 than with x_2. The "keying" of d_2 to d_1 is not surprising in view of the high mobility of NH_3 in the galleries of laterally contiguous stage-1 and stage-2 regions, as would exist in the Daumas-Hèrold (DH) model[43] of the layer structure of GIC's which is shown schematically in Fig. 13. In the DH model each gallery contains some intercalant which, however, may show lateral inhomogenities in its distribution. Macroscopic regions of different stage are separated by kink dislocations as shown in Fig. 13. But an NH_3 molecule can dynamically sample contiguous stage-1 and stage-2 regions while still remaining in the same gallery.

The expanded stage-1 sandwich (d_{s_1}) imposes both a dynamic and static strain on the stage-2 sandwich (d_{s_2}) resulting in a small decrease in d_{s_2} as compared with d_{s_1} ($d_{s_1}-d_{s_2}=0.05$ Å). In fact, the strain between the stage-1 and stage-2 regions, as measured by the difference between d_2 and d_1, remained constant over the pressure range $0.1<P_{NH_3}<6.5$ atm, with $d_2-d_1=3.30$ Å. The extrapolated value of $d_2=9.93$ Å (see dashed line in Fig. 5) also indicates that this strain persists even at $P_{NH_3}=9.5$ atm (of course the extrapolation assumes that stage 2 still exists at that pressure). It is interesting to note that higher-stage mixed-phase K-NH_3 GIC's also show the same difference between d_{n+1} and d_n for stage n. For example, Fig. 10 shows the room-temperature x-ray diffraction pattern of $KC_{36}+NH_3$, which indicates a stage-1 and stage-2 mixture with $d_1=6.638$ Å, $d_2=9.938$ Å, and $d_2-d_1=3.300$ Å. Figure 14 shows that the room-temperature ($00l$) x-ray diffraction pattern of $KC_{48}+NH_3$ also indicates a mixed stage compound

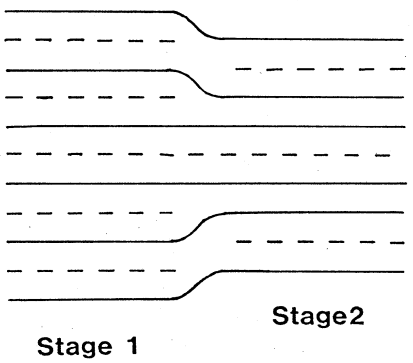

FIG. 13. Daumas-Hèrold model (Ref. 43) of laterally contiguous layers of stage-1 and stage-2 regions present in a mixed stage graphite intercalation compound.

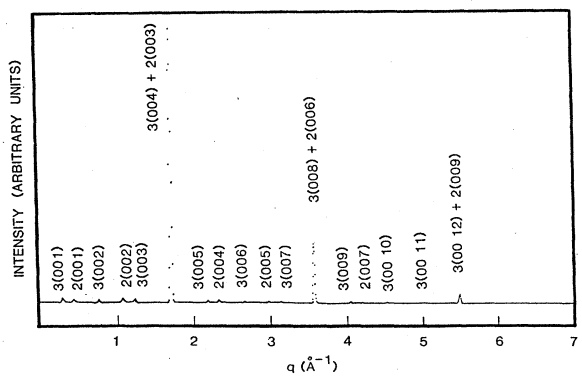

FIG. 14. Room-temperature ($P_{NH_3} \approx 9.5$ atm) ($00l$) x-ray diffraction pattern of $KC_{48}+NH_3$ liquid. The notation is the same as that of Fig. 3.

which in this case is composed mostly of stage-2 material ($d_2 = 9.984$ Å) with some stage-3 admixture ($d_3 = 13.29$ Å). Again, we find that $d_3 - d_2 = 3.306$ Å.

It is clear from the above discussion that for mixed-phase K-NH_3 GIC's which are composed of 2 stages, n and $n+1$, the lower stage n imposes a strain on the higher stage $n+1$, and that this strain is insensitive to variations in P_{NH_3}. Moreover, the sandwich thickness of the stage-n phase is essentially independent of that strain. To support this point we note that the value of d_{s_2} for $KC_{48}+NH_3$ is 6.634 Å and is identical to the strain-free value of d_{s_1} for $K(NH_3)_{4.33}C_{24}$.

IV. SUMMARY AND CONCLUDING REMARKS

We have found that as P_{NH_3} is lowered, the stage-1 $K(NH_3)_{4.33}C_{24}$ ternary GIC evolves to a mixed-phase stage-1 $K(NH_3)_{x_1}C_{y_1}$ and stage-2 $K(NH_3)_{x_2}C_{y_2}$ system, with unexpected variations of the carbon/potassium ratios y_n (for stage n) with P_{NH_3}. At $P_{NH_3} = 9.5$ atm we find that $x_1 = 4.33$ and $y_1 = 24$ and estimate that $y_2 > 37$ and $x_2 > 3.2$. As the ammonia pressure is lowered, both y_1 and y_2 decrease and at $P_{NH_3} \sim 10^{-2}$ atm could be extrapolated to $y_1 = 12$ and $y_2 = 28$, which is consistent with the stoichiometry of compounds prepared by Rudorff and Schultze,[18] namely stage-1 $K(NH_3)_{2.0}C_{12}$ and stage-2 $K(NH_3)_{2.0}C_{28}$.

It was found that the sandwich of stage 1 imposed an elastic strain on the sandwich of stage 2 such that $d_{s_1} - d_{s_2} = 0.05$ Å and that this strain was insensitive to variations in P_{NH_3}. Both d_{s_1} and d_{s_2} were found to depend on the variations of x_1 with P_{NH_3}, which was fit to a Fowler-Guggenheim equation for adsorption.

From x_1 versus P_{NH_3} in Eq. (11) and the independently determined value of $k_A/k_K = 0.65$, we fit the d_1-versus-P_{NH_3} data in Fig. 4 using Eq. (18) with only two adjustable parameters. The resultant fit constitutes excellent agreement between theory and experiment. Both the P_{NH_3} data in Fig. 4 using Eq. (18) with only two adjustable parameters. The resultant fit constitutes excellent agreement between theory and experiment. Both the sandwich thickness of the NH_3 GIC and the charge exchange f could be independently extracted from the fit to d_1 versus P_{NH_3}. The deduced value of $f = 0.95$ is in reasonable agreement with values obtained from other measurements. The deduced charge exchange can be brought into closer agreement with reflectivity[16] and NMR (Ref. 15) measurements by incorporating multiple-electron solvation mechanisms into Eq. (16).

The physical origin of our results may be separated into three major effects. First, as NH_3 is added to the interlayer space containing K^+ ions, an expansion results from the size difference of NH_3 relative to K^+ (i.e., $d_A/d_{K^+} > 1$). Second, as NH_3 is ingested, some of the charge originally donated to the carbon layers is extracted back into the K-NH_3 layer, concurrent with electron-cage formation, and is delocalized. Third, much of the delocalized charge resides near the potassium ions and increases their effective radii. This increased potassium radius generates additional elastic energy causing an increase in d_{s_1}.

The fractional increase of our stage-1 $K(NH_3)_{4.33}C_{24}$ ($d_{s_1} = 6.633$ Å) from Rudorff and Schultze's stage-1 $K(NH_3)_{2.0}C_{12}$ ($d = 6.5$ Å) is 2%, which is very close to our estimate of the elastic contribution of the charge exchange term in Eq. (18) and suggests that the difference is entirely due to an elastic-charge transfer coupling.

Finally, the experimental results from several measurements[11–13,19] can also be separated into three important effects. First, there is a significant extraction of charge from the graphite layers ($f \approx 1.0$ to $f \approx 0.80$) to the intercalant layer due to intercalated NH_3, attributable to electron solvation. Second, the K-NH_3 intercalant forms a 2D liquid in the graphite gallery with the K ion forming a planar fourfold-coordinated cluster with the NH_3 molecule and the excess NH_3 molecules [0.33 per $K(NH_3)_4$ cluster at $P_{NH_3} = 0.5$ atm] lying in the plane defined by those clusters. Third, the relative potassium-ammonia concentration can be continuously varied from 19 to 100 MPM with indications (see Fig. 8) that higher stages may provide a lower in-plane potassium density than that corresponding to $y_1 = 24$ for stage 1. This would leave additional room for NH_3 and yield a lower minimum concentration.

These results for the K-NH_3 GIC are consistent with the formation of a 2D metal-ammonia solution in the gallery of graphite. Higher stages may provide the means of accessing the dilute region < 0.1 MPM, in which case the K-NH_3 ternary GIC's could be a novel and intrinsically interesting system for studying the 2D nonmetal-metal transition.

ACKNOWLEDGMENTS

We gratefully acknowledge numerous fruitful discussion with J. L. Dye, S. D. Mahanti, and S. K. Hark, who also assisted in the data acquisition and analysis. Thanks are due to A. W. Moore for providing the HOPG used in this study. This work was supported by the NSF under Grant No. DMR 82-11554.

[1]S. A. Safran, Phys. Rev. Lett. **44**, 937 (1980).
[2]S. E. Millman and G. Kirczenow, Phys. Rev. B **26**, 2310 (1982).
[3]P. Hawrylak and K. R. Subbaswamy, Phys. Rev. B **28**, 4851 (1984).
[4]S. A. Safran and D. R. Haman, Phys. Rev. B **22**, 606 (1980).
[5]S. A. Safran and D. R. Haman, Phys. Rev. Lett. **42**, 1410 (1979).
[6]R. Clarke, N. Wada, and S. A. Solin, Phys. Rev. Lett. **44**, 1616 (1980).
[7]C. D. Fuerst, J. E. Fischer, J. D. Axe, J. B. Hastings, and D. B. McWhan, Phys. Rev. Lett. **50**, 357 (1983).
[8]K. D. Woo, W. A. Kamitakahara, D. P. DeVincenzo, D. S. Robinson, H. Mertwoy, J. W. McViker, and J. E. Fisher, Phys. Rev. Lett. **50**, 182 (1983).
[9]A. Metrot and J. E. Fischer, Synth. Met. **3**, 201 (1981).
[10]D. A. Neuman, H. Zabel, J. J. Rush, and N. Berk, Phys. Rev. Lett. **53**, 56 (1984).
[11]A. Hèrold, in *Proceedings of the International Conference on the Physics of Intercalation Compounds,* edited by L. Pietronero and E. Tosatti (Springer, New York, 1981), p. 7.
[12]S. K. Hark, B. R. York, S. D. Mahanti, and S. A. Solin, Solid State Commun. **50**, 545 (1984).
[13]S. A. Solin, Y. B. Fan, and B. R. York, Bull. Mater. Res. Soc. (to be published).
[14]J. L. Dye, Prog. Inorg. Chem. **32**, 327 (1984).
[15]J. C. Thompson, *Electrons in Liquid Ammonia* (Clarendon, Oxford, 1976).
[16]*Electrons in Fluids: The Nature of Metal-Ammonia Solutions,* edited by J. Jortner and N. R. Kester (Springer, New York, 1973).
[17]J. C. Thompson, Rev. Mod. Phys. **40**, 704 (1968).
[18]W. Rudorff and E. Schultze, Angew. Chem. **66**, 305 (1954).
[19]H. Resing, B. R. York, and S. A. Solin (unpublished).
[20]D. Hoffman, A. M. Rao, G. L. Doll, P. C. Eklund, B. R. York, and S. A. Solin, Bull. Mater. Res. Soc. (to be published).
[21]A. Hèrold, Bull. Soc. Chim. Fr. 999 (1955).
[22]R. R. Dewald and J. H. Roberts, J. Phys. Chem. **72**, 4224 (1968).
[23]J. W. McBain and A. M. Baker, J. Am. Chem. Soc. **48**, 690 (1926).
[24]*International Critical Tables of Numerical Data, Physics, Chemistry, Technology,* 1st ed., edited by E. W. Washburn (McGraw-Hill, New York, 1928), Vol. III.
[25]*Handbook of Chemistry and Physics,* 55th ed., edited by R. C. Weast (Chemical Rubber Co., Boca Raton, Florida, 1974).
[26]N. Akuzawa, M. Ikeda, T. Ameniya, and Y. Takahashi, Synth. Met. **7**, 65 (1983).
[27]P. Chow and H. Zabel, Synth. Met. **7**, 243 (1983).
[28]R. Fowler and E. Guggenheim, *Statistical Thermodynamics* (Cambridge University Press, Cambridge, England, 1949).
[29]J. D. Jackson, *Classical Electrodynamics,* 2nd ed. (Wiley, New York, 1974).
[30]A. H. Narten, J. Chem. Phys. **49**, 1692 (1968).
[31]N. A. W. Holzwarth, S. Louie, and S. Rabii, Phys. Rev. Lett. **47**, 1318 (1981).
[32]J. R. Dahn, D. B. Dahn, and R. R. Haering, Solid State Commun. **42**, 179 (1982).
[33]T. Enoki, M. Sano, and H. Inokuchi, J. Chem. Phys. **28**, 4 (1983).
[34]D. A. Copeland, N. R. Kestner, and J. Jortner, J. Chem. Phys. **53**, 3741 (1975).
[35]N. F. Mott and E. A. Davis, *Electronic Processes in Non-Crystalline Materials* (Clarendon, Oxford, 1971).
[36]T. A. Beckman and K. S. Pitzer, J. Phys. Chem. **65**, 1527 (1961).
[37]J. L. Dye, Pure Appl. Chem. **49**, 3 (1977).
[38]W. A. Siddon, J. W. Fletcher, R. Catterall, and F. C. Sopchyphyn, Chem. Phys. Lett. **48**, 584 (1977).
[39]G. Dresselhaus, R. Al-Jishi, J. D. Axe, C. F. Majkrzak, L. Passell, and S. K. Satija, Solid State Commun. **40**, 229 (1981).
[40]*Landolt-Börnstein Numerical Data and Functional Relationships in Science and Technology,* edited by K. H. Hellwege (Springer, New York, 1979), Vol. II.
[41]O. J. Kleppa, J. Chem. Phys. **18**, 1331 (1950).
[42]C. Kittel, *Introduction to Solid State Physics,* 2nd ed. (Wiley, New York, 1957).
[43]N. Daumas and A. Hèrold, Bull. Soc. Chim. Fr. **5**, 1598 (1971).